

AUTOMATIC QUANTIFICATION OF CELL VIABILITY IN HIPPOCAMPAL
ORGANOTYPIC CULTURES

By

APARNA KANNAN

A thesis submitted to the

Graduate School-New Brunswick

Rutgers, The State University of New Jersey

In partial fulfillment of the requirements

For the degree of

Masters of Science

Graduate Program in Biomedical Engineering

Written under the direction of

DAVID SHREIBER

And approved by

New Brunswick, New Jersey

October 2014

ABSTRACT OF THE THESIS

Automatic Quantification of Cell Viability in Hippocampal Organotypic Cultures

By APARNA KANNAN

Thesis Director:

DAVID SHREIBER

Traumatic Brain Injury (TBI) is a leading cause of disability with many different types of forces. Because the brain is made of up interconnected nerve cells, injury from one area of brain can easily spread throughout the rest of the brain. In order to study this effect in this paper, we use hippocampal organotypic cell cultures. To analyze how secondary and further injury is spread in the brain due to TBI, specific regions of interest are outlined using bright-field microscopy images and analyzed for cell death through fluorescent images. Because of the bias in segmenting these specific regions, and the darkening of bright-field images from necrosis, there is a need for the development of an automatic cell viability analysis method. We first create silhouette masks identifying the area of the hippocampus within the bright-field images. Then, we align these masks of these images between two time points – one

before experimentation and another 24 hours after lab experimentation - using Mattes Mutual Information registration to help analyze corresponding regions between time points. We also use relative intensity gradients and contrast enhancement to help isolate the specific regions of interest within the hippocampus, and then aligned the regions of interest between time points using the transformation discovered through the registration process. Finally, we look within these extracted regions for cell viability in fluorescent images taken after experimentation and calculate the ratio between the area of the fluorescent region extracted and the area of the segmented region. Comparing the results from this method with manual segmentation by experienced users, we discover an average of 12% error in segmentation and 2% error in registration. The overall method took an average of 7 minutes per image, which compared to the time it takes complete manually, allows users to conserve time and prevent user-to-user bias in segmentation.

Acknowledgements and/or Dedications

I would like to thank Dr.Shreiber and lab for providing his resources/skills, which assisted this work in its use.

Contents

Abstract.....	ii
Acknowledgements and/or Dedications.....	iv
Introduction.....	1
Rationale.....	2
Aims and Objectives	4
Methods.....	6
Data set.....	6
REGISTRATION PHASE.....	6
Segmentation of the Hippocampus from Background.....	6
Comparing Mono-model vs Multi-Model Metrics.....	9
Registration: Progression vs Binary Branch and Order	10
Affine Progression	12
Affine Binary Bank.....	12
Rigid Progression/ Binary Bank	12
Similarity Progression/Binary Bank.....	13
SEGMENTATION PHASE	13
CALCULATING CELL DEATH.....	15
Results/Discussion	16
REGISTRATION RESULTS.....	16
Affine Progression	17

Affine Binary Branch	19
Rigid Progression	20
Rigid Binary Branch	22
Similarity Progression.....	24
Similarity Binary Branch	26
SEGMENTATION PHASE:	28
Combining Segmentation and Registration	33
Fluorescence measurements	34
Conclusion:	38
Appendices.....	40
References:	40
Bibliography	41

Table of Illustrations

Figure [1]. The regions of a rat hippocampus, include the dentate gyrus (shown as DG), CA3, CA1. Taken under brightfield microscope.....	1
Figure [2]. This shows the process of extracting the hippocampus from image. [a]. Original image [b]. Binary gradient mask [c]. mask after dilation [d]. filling in the mask's holes [e]. segmented with largest area [f]. smoothing segmented image [g]. Outlining points from the border of segmented image on original image [h]. outlining points from border of segmented image	7
Figure [3]. This diagram describes how one cycle/step/iteration of the registration process..	9
Figure [4]. The chart shown above shows the breakdown of the experiments..	10
Figure [5]. The following graph shows the % difference between the registered and the final image for 200 steps in intervals of 20 steps to help understand how the multimodal metric works.....	11
Figure 6 Segmentation Process	15
Figure 7 Fluorescence Measurement Process Shown.....	16
Figure [8]. Results from tests on Affine Progression method for 5 images	17
Figure [9]. Overlapping registered image on reference image for Affine Progression Method at various time points.....	18
Figure [10]. Results from tests on Affine Binary Branch method for 5 images.....	19
Figure [11]. Overlapping registered image on reference image for Affine Binary Branch Method at various time points.....	19
Figure [12]. Results from tests on Rigid Progression method for 5 images.	20
Figure [13]. Overlapping registered image on reference image for Rigid Progression Method at various time points.....	21

Figure [14]. Results from tests on Rigid Binary Branch method for 5 images.....	22
Figure [15]. Overlapping registered image on reference image for Rigid Binary Branch Method at various time points.....	22
Figure [16]. Results from tests on Similarity Progression method for 5 images.....	24
Figure [17]. Overlapping registered image on reference image for Similarity Progression Method at various time points.....	24
Figure [18]. Results from tests on Similarity Binary Branch method for 5 images.	26
Figure [19]. Overlapping registered image on reference image for Similarity Binary Branch Method at various time points.....	26
Figure 20 Raw Bright-field Images of 14 slices from 4 different rat brains.....	28
Figure 21 “Concentrated” Region of 14 slices from Figure 20.....	28
Figure 22 10 Hz Butterworth Filter and 2x2 Median Filter applied on Original Slices from Figure 18.....	29
Figure 23 Images result from difference between Figure 21 and Figure 22 are extracted. The resulting images are contrast enhanced such that 1% of values are saturated at high and low intensities.	29
Figure 24 CLAHE contrast enhancement on resulting images of Figure 23. All regions outside the concentrated region are ignored.....	30
Figure 25 Scale result from CLAHE to maximum intensity	30
Figure 26 20x20 Median Filter to fill in small gaps in extracted regions. A 10 pixel radius disk structuring element is then used to separate loosely connected regions.....	31
Figure 27 Different Connected Components Labeled.....	31

Figure 28 My Segmentation vs Manual Segmentation.....	32
Figure 29 Target registration error.....	33
Figure 30 Cell Death Measurements for 14 slices from 4 different rat hippocampi.....	34
Figure 31 Overlap of Fluorescence Image after threshold and binary step and automatically segmented regions	35
Figure 32 Overlap of Fluorescence Image after threshold and binary step and manually segmented regions.....	35
Figure 33 Cell Death Measurements for 14 slices from 4 different rat hippocampi: Automatic vs 2 Manual Experts.....	36
Figure 34 Efficiency of automated process from beginning of registration phase until end of cell viability measurement phase.....	36

Introduction

Traumatic Brain Injury (TBI) is a leading cause of disability and can be triggered by various events such as through impact forces, penetration forces, or deceleration forces during a vehicular accident or fall (reviewed in Laurer et al., 2000). By replicating different brain damage scenarios, in vivo models can help us understand how initial brain tissue injury leads to further brain damage. Unfortunately, the majority of current trauma in vivo models are induced by injury through impact or penetration, despite over 50% of trauma accidents occurring from deceleration forces of automotive accidents (Sosin et al., 1979; Bruns and Hauser, 2003). Additionally, the brain consists of networks/neural circuits that are interconnected so damage from one area easily spreads to others (Faden et al., 1989). Because organotypic hippocampal slice cultures consist of similar networks of neurons and glia, they can be used to understand the complex cascade of events following brain damage

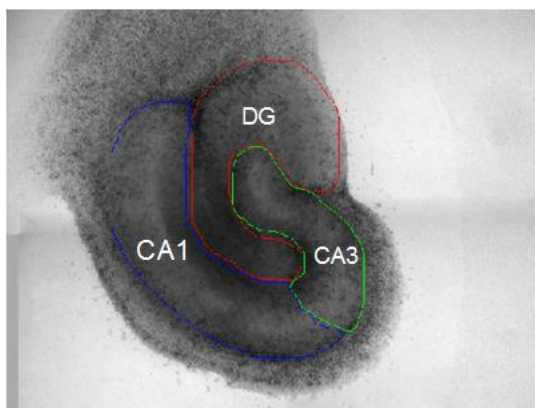


Figure [1]. The regions of a rat hippocampus, include the dentate gyrus (shown as DG), CA3, CA1. Taken under bright-field microscope.

(Morrison III, B et al. 2005)

TBI can lead to different neurological and cognitive problems, such as those related to the function of the hippocampus (Bramlett et al., 1997; Levin, 1998). The hippocampus is an organ which plays a huge role in memory

and spatial navigation, and is located in the medial temporal lobe of the brain. Damage to this area can cause memory loss and disorientation. The main layers of the hippocampus are the dentate gyrus (DG), and two cornu ammonis (CA) layers, identified as CA3 and CA1, as shown in Figure [1]. Because the flow of information signals in a hippocampus involves

interaction of cells starting from the dentate gyrus, followed by the CA3 layer, and then through the CA1 layer, it is key to keep track of the cell viability during experimentation of these regions. To track damage to the organ, scientists stain the organ slices with fluorescent markers, such as propidium iodide, during experimentation (Morrison III, B et al. 2005). Based on the level of fluorescence, scientists can use imaging techniques to view the fluorescence images and measure cell viability between different time points. Bright-field images, before experimentation, can help us identify the location of these regions, which can then be transposed onto fluorescent images to calculate the cell viability in those areas alone. Unfortunately, because of the tissue's molecular interactions with the slide surface and small stresses applied during experimentation, slice images are not necessarily aligned in the same way between time points. Molecular interactions may cause edges of tissue to contract or expand making it appear slightly smaller or larger, while stresses slightly deform the tissue. Because of this, images need to be aligned before layers can be transposed and measurements can be taken on the fluorescent images. Once the three regions of interest – CA1, CA2, and DG layer – are segmented, image registration methods can help align the images between time points and facilitate identifying the location of the layers between time points.

Rationale

Segmentation algorithms is an important step to analyzing medical images. There are three main types of segmentation, defined by the level of user interaction. Supervised segmentation, or manual segmentation, involves the user, usually a trained expert, delineating the regions of interest and applying analysis. Metamorph and ImageJ are computer programs that include software allowing for manual segmentation and definition of regions of interest for further analysis. Results from this segmentation are referred to as ground truth, but

unfortunately can be prone to variability and bias, leading to less reproducible analysis and diagnosis, as well as time consuming. Semi-supervised and unsupervised hippocampus segmentation algorithms, involving little or no user input, were created with MRI images (Minjeong et. al 2013; Kai-kai et. al 2011) using deep unsupervised learning and shape models, respectively. Additionally, automatic cell segmentation algorithms for bright-field images (Rehan Ali et. al 2010; Tscherepanow M 2008) exist, using image gradients and other features. Using different imaging programs and functions, i.e Digital Image Correlation (DIC) technique (Wang et al., 2002), regions of interests (ROI), such as the hippocampus layers in this paper, are outlined and relevant measurements are taken, such as area, range of intensities, etc. Despite there being previous works related to segmentation of the hippocampus in brain MRI slice images and of individual cells from bright-field images, there isn't any work related to the segmentation of the particular structures within the hippocampus from bright-field images.

Unfortunately, due to necrosis, or the death of cells in an organ due to forces external to cells such as injury or blood supply failure, parts of the image under bright-field microscopy darken. This makes it harder to locate the layers on images during or after experimentation to calculate feature values, such as cell viability. Occasionally, the tissue's interaction with the slide surface and stresses applied during experimentation induce small deformations in the image in the tissues that must be taken into account for precise analysis. Therefore using only segmentation algorithms will not help provide enough information for analysis. We need to use the segmentation method from images taken before segmentation and use it to finding the corresponding regions in the image of the hippocampus taken after experimentation. Just like segmentation algorithms vary based on level of user input, registration algorithms are also different for different levels of user input. Aligning and

outlining layers manually presents person-to-person bias as well as consuming large amounts of time with large data sets. Therefore it is important to create an automatic method that can help save time as well as align the images and identify the specific layers between different time points to precisely calculate the desired features, such as cell viability, within the regions of interest.

Aims and Objectives

Our main objective is to measure the level of cell death within the three layers of the hippocampus. Once image pairs are registered, or aligned, and hippocampal layers are identified, we can better identify the layers on the 24-hour time stamped image and quantify cell viability based on how the images were transformed, or aligned, between the initial and 24-hour time points. Registration is based on coordinate transformations including translations and rotations, due to changes in frame of reference and other factors such as dilation or scaling due to tissue spreading/contracting. The specific types, monomodal and multimodal, refer to how the images are acquired: monomodal methods register images acquired by same scanner/sensor type while multimodal methods register images acquired by different scanner/sensor types. (Fitzpatrick). Multimodal registrations also can be used when images differ widely in intensities. Segmentation is based on pre-processing techniques such as contrast limited adaptive histogram equalization and intensity based features. After applying a threshold on the intensities of the fluorescent images after experimentation, cell viability will be measured based on the ratio of the number of colored pixels to the area of the segmented area.

The first aim will be to register, or align the hippocampus from the image taken before experimentation to the hippocampus of image taken 24 hours after experimentation.

To do this, we prevent background image information from affecting the registration, it is necessary to isolate the hippocampus in the image from its background so we can clearly lineate the hippocampus for registration. A binary silhouette of the hippocampus image is extracted where all parts of the hippocampus are colored with white pixels and the background is colored in black pixels. Once we can clearly see the shape of the hippocampus, we would test out different methods of using the multimodal registration metrics to see which best aligns the initial and 24-hour image of the hippocampus with each other, based on precision and time-efficiency. Finally after finding the best methods for the image registration, we would compare this method with manual alignment of images done using Metamorph program currently.

The next aim involves finding an optimum algorithm for segmenting the layers within the hippocampus and identifying them as either CA1, CA3, or DG layer. We take advantage of the intensity based information given by the bright-field microscopy images taken before experimentation to identify these layers. We then apply the effective transformation extracted from the registration phase to transform these extracted layers to their corresponding locations of the layers in the image taken 24 hours after experimentation.

Finally, we will measure the cell death within these extracted and appropriately aligned layers of the hippocampus from the fluorescent images taken 24 hours after experimentation. Because these images are of organ slices, the images are pre-processed by applying a threshold on the relative intensities of the fluorescent images, measuring the total number of pixels within the segmented regions, and calculating the ratio between the sum and the area of the segmented region.

Since manual registration and delineation of hippocampi layers for each initial and 24-hour image consumes time with variable outcomes due to errors like person-to-person and image-to-image bias in determining how aligned a pair of images are, an automatic registration and cell viability quantification method is necessary to align images with higher precision and accuracy and time-efficiency.

Methods

Data set

Our data set consists of bright-field hippocampal slice images to help us identify the location of the hippocampal layers, and fluorescent hippocampal slice images to help us calculate cell viability. Each set of images are divided into two groups of 45 hippocampal image samples each, representing two time points: the initial images taken before experimentation and the final images taken 24 hours after the start of the experiment. In this paper, images taken before experimentation will be referred to as the pre set, while the images taken 24 hours after experimentation will be referred to as the post set.

REGISTRATION PHASE

Segmentation of the Hippocampus from Background

To prepare for the registration process and remove noise from the differences in relative intensities of the pixels between the pre and post hippocampus image sets, the hippocampus in each bright-field image is isolated, or segmented, from its background.

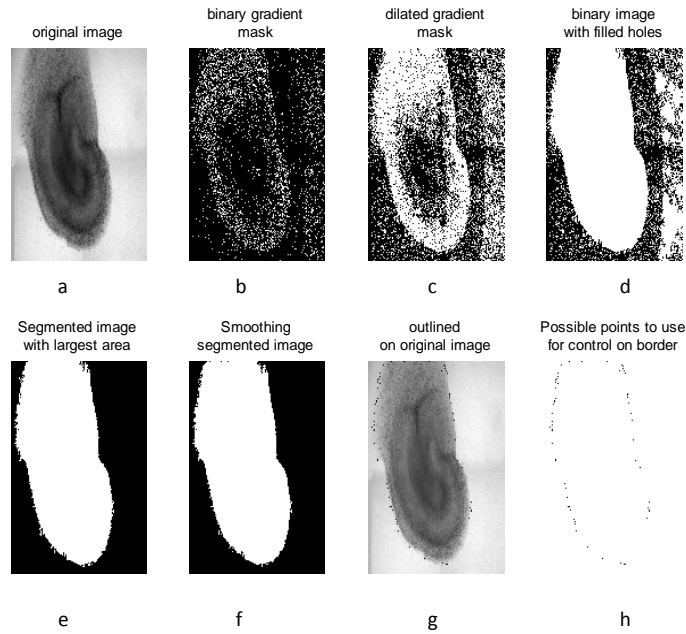


Figure [2]. This shows the process of extracting the hippocampus from image. [a]. Original image [b]. Binary gradient mask [c]. mask after dilation [d]. filling in the mask's holes [e]. segmented with largest area [f]. smoothing segmented image [g]. Outlining points from the border of segmented image on original image [h]. outlining points from border of segmented image

To

accomplish this, we first created and fine-tuned a binary mask.

FIGURE [2a]

shows a typical bright-field image before

experimentation.

Noting the difference

between the intensities of pixels that outlines and covers the area of the hippocampus and the background outside the area of the hippocampus, we used a built in edge method with the Sobel operator. This method created edges, by drawing line segments on the image where there was a high intensity gradient, according to a threshold calculated based on the distribution of pixel intensities. Edges whose gradients are not stronger than this threshold value are not displayed. Since the intensities of pixels within the borders of the hippocampus vary as well, we fine-tuned the gradient-based image by applying a new threshold that is half of the initial threshold to account for more edges of the hippocampal slice in the image, while including a minimal number of edges outside the area of the hippocampus. Edges extracted from the background due to shadows will be removed in later steps. This step produces a binary gradient mask of the hippocampus image as shown in FIGURE [2b].

Despite decreasing the threshold value and increasing the number of edges within the area of the hippocampus, a clear outline of the hippocampus is not clear from the given image result. There are gaps between the lines denoted as edges in the binary gradient mask. This problem is solved by dilating the binary gradient mask using linear structuring elements which join edges that are at a certain angle and distant from each other. In FIGURE [2c], edges are connected using vertical structuring elements (edges facing 90 degrees counterclockwise from the positive horizontal axis) followed by a horizontal structuring element (facing zero degrees from the positive horizontal axis) another edge, in addition to being 3 pixels away from each other. The outline of the possible hippocampus becomes clearer from the dilation. To cover the entire portion of these regions, we fill in the holes of each detected closed region as shown in FIGURE [2d].

Based on observation of all the images, the hippocampus can be clearly differentiated by the estimated area it covers. To segment the hippocampus from other displayed noisy regions, we removed all regions of interest that have fewer than 80,000 pixels. This value was tested to be the general number of minimum pixels to separate it from the noisy objects in all of the images from the bright-field data set. By filtering out the noisy objects, the hippocampus is segmented from the background as shown in FIGURE [2e]. Finally to make the image look smoother, the image is eroded twice with a diamond structuring element. The resulting image is shown in FIGURE [2f] and labeled as the final binary silhouette used for registration.

FIGURES [2g] and [2h] show how closely the outline of the segmented area overlaps with the original image and how these points give an overall idea of the hippocampus shape.

Comparing Mono-model vs Multi-Model Metrics

In this paper, we used an intensity-based automatic image registration algorithm.

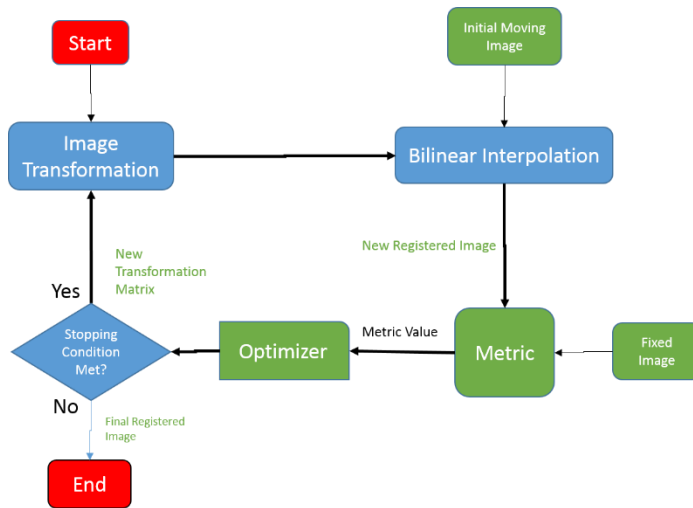


Figure [3]. This diagram describes how one cycle/step/iteration of the registration process. Starting with a type of transformation (affine, rigid, etc), and the moving image to be registered, the metric and optimizer work together to estimate the registered image. Changing the metric’s properties will change the registered image. This cycle is repeated until the stop condition is met.

Image registration requires four main types of inputs: a pair of images, a metric, an optimizer and a transformation type. The metric helps define a similarity metric that informs the program about how similar images are for registration accuracy. The optimizer defines a method to maximize or minimize the similarity metric, and checks

for a stop condition – when the process has reached a specific number of iterations or a point of diminishing returns. The transformation type defines the type of 2-D transformation that brings the misaligned image (called the moving image) into alignment with the reference image (called the fixed image) (Shi et. al 2014). The overall registration process is outlined in FIGURE [3].

There are two different metrics, each suited for a specific type of registration mode. The Mean-Squares metric works for mono-modal images, which are captured from the same scanner/source, and computes the element-wise difference between two input images (Ulssys et. al 2010). The Mattes mutual information metric works for multi-modal images, whose sources are from different scanners/sources, and uses “information theoretic techniques for measuring how related two variables are. These algorithms use the joint probability distribution to measure how likely a sample of pixels from one image match the

same sample in another image (Ulssys et. al 2010). To define the stop condition as the number of maximum iterations and control the registration step-wise, the multi-modal is chosen as more preferable for this paper.

Registration: Progression vs Binary Branch and Order

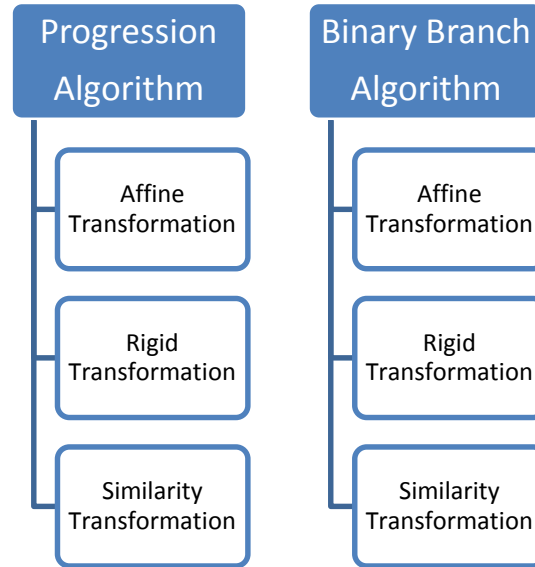


Figure [4]. The chart shown above shows the breakdown of the experiments. To run an experiment, an algorithm, a transformation type and a set of images for reference in registration should be picked. The two main algorithms used are called Progression and Binary Branch. The transformation types chosen are affine, rigid and similarity

As FIGURE [4] shows, the tested set methods are broken into different groups – the type of algorithm, the type of transformation, the image that controls the registration per step, and the image that is chosen as the

reference (fixed image). A Progression algorithm is defined as a parent (moving) image being registered to a reference image by incrementing one of the metric's property MaximumIteration#, defined by the number of maximum cycles, described by Figure [3] previously, the registration process takes the parent image to align with the fixed reference image.

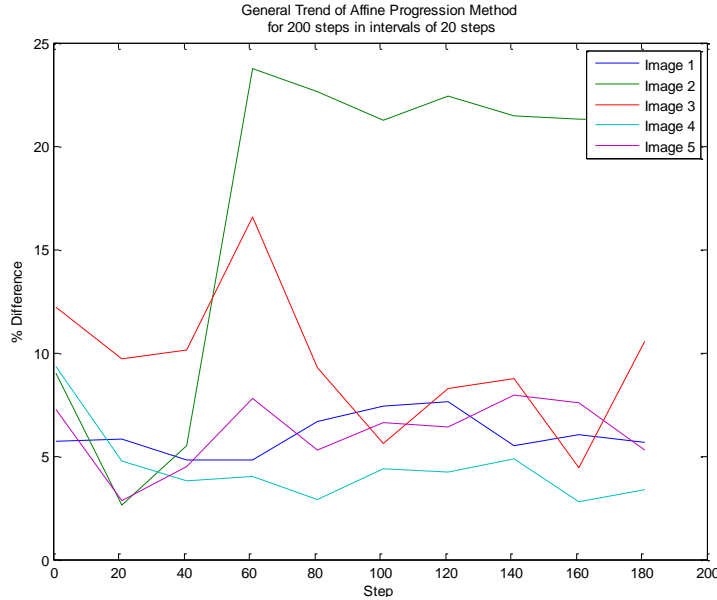


Figure [5]. The following graph shows the % difference between the registered and the final image for 200 steps in intervals of 20 steps to help understand how the multimodal metric works. Steps also define the number of iterations or cycles (from Figure [2]) the process went through. This number is defined in the property MaximumIteration#.

Due to some sharp differences between transformed images during registration, a new algorithm, incorporating a similar methodology of the Means-Square metric, is created to control the

differences between images per registration step from changing sharply. The Binary Branch algorithm is defined by a parent (moving) image being registered to a final (fixed) image, where the parent image changes based on the result of the previous registration step. Suppose that P represents the moving image to be registered (parent), C represents the image that results from P's registration, after one iteration, and F represents the fixed reference image. If $|C-F| < |P-F|$, or the absolute value of the element-wise difference between the registered image and final image is less the absolute value of the difference between the parent image and the final image, then C is the new parent and becomes P for the next registration step, and the MaximumIteration# property is set back to 1. If $|C-F| > |P-F|$, then P stays as the parent image for the next registration step and the MaximumIteration# parameter is incremented by 1.

Affine Progression

To cover all the aspects of transformations, we begin with the most general types of transformations – affine. The affine transformation accounts for translation, rotation, scale and shear. To better understand how the registration metric works, 5 pairs of image silhouettes are tested for a maximum of 80 steps. This value is based on Figure [5] where 200 iterations, in intervals of 20 iterations, were tested. All the main information in the precision and efficiency of the registration are given within the first 80 steps. Any additional steps would increase the cost of time in comparison to precision of the registered results.

Affine Binary Bank

To prevent large differences from step to step, it was necessary to understand how the transformation matrix for the image is created. Unfortunately, due to privacy, the code for the transformation matrix calculation was unavailable. Therefore, to try and control the sharp changes in difference between silhouettes, the Binary Branch algorithm was applied with Affine Transformation.

Rigid Progression/ Binary Bank

Due to the large amount of time the affine transformation methods consumed, and the large differences between silhouettes of the parent and final image, a simpler type of transformation is tested. This would also match the method lab members use to manually align the images – through pure translation and rotation - more. For similar reasons as above, the Binary Branch algorithm was also attempted with rigid transformation.

Similarity Progression/Binary Bank

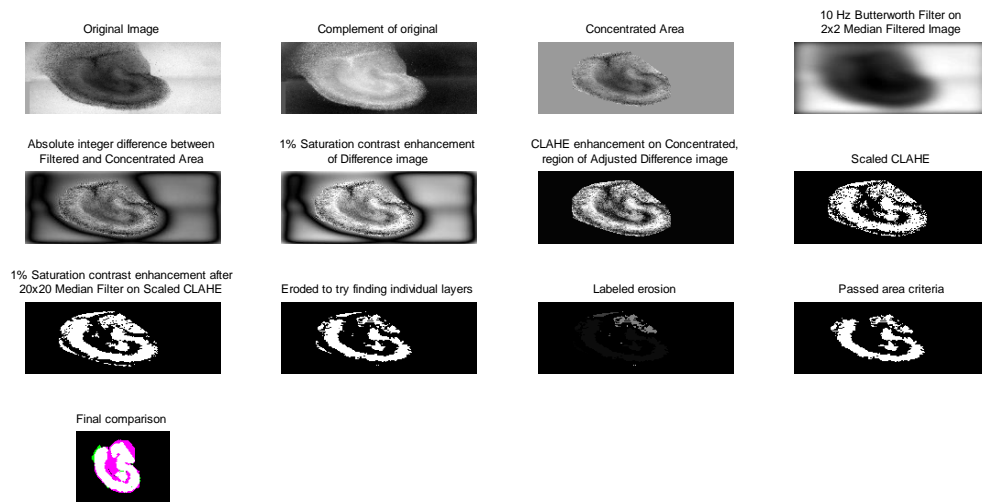
To account for possible tissue contracting/expansion, we decided to attempt using the similarity transformation type which accounts for the translation, rotation and scaling of the image. The progression and Binary Branch algorithms were tested as described before.

SEGMENTATION PHASE

The next phase of the project is to identify the layers within the hippocampus slices. We identify them using the bright-field images of hippocampus slices before experimentation because the layers are clearly visible, as opposed to the slices after experimentation. The first step in the segmentation process involves extracting the region of the hippocampus that surrounds the layers we are interested in. One clear feature in most of the bright-field microscopy images is the dark region shaped like a curvy T between the CA1 and DG layers, associated with the hippocampal sulcus (FIGURE [2a]), and the thin dark region appearing as an outer perimeter around the CA1,CA3,and DG layer. Inverting the original image allows the dark regions to become bright regions. By inverting around 20 bright-field images, we discover in order to obtain a more precise border of the layers, we need to keep at least the top 30% of the intensities of the inverted images. By extracting the top 30% of the intensities, and taking the convex hull of the extract, we are able to create a mask that, once applied on the original bright-field image, will help identify a more precise estimate of where the layers of interest are located. The image resulting from this process is referred to as the concentrated region in Figure 6.

Once we have this concentrated region, we apply a second order Butterworth filter, with a cutoff frequency of 10 Hz, on the original image to get a smoothened image of hippocampi that results in a relative contour map image for groups of gradually increasing intensities

from the center of the hippocampus. This cutoff frequency was determined to provide the best difference between the dark center of the hippocampus and the light gray regions of interest, after testing out several different cut off frequencies from 5Hz to 20Hz. After 10Hz, the bright-field image began to show unnecessary noise that affected the identification of the inner boundary of the layers. We obtain a difference image by taking the absolute integer difference between the Butterworth filtered image and the concentrated region. The gradual increase in the Butterworth filter image scale intensities within each contour region of the Butterworth filter, identifying pixels with higher probabilities of being within the regions of interest (hippocampus layers). After this, we increase the contrast such that 1% of data is saturated at low and high intensities followed by a contrast limited adaptive histogram equalization to enhance the areas with highest probability of being located in the regions of interest. While histogram equalization increases global contrast by spreading out the most frequent intensity values in the image, adaptive histogram equalization applies histogram equalization to each distinct section of an image. Unfortunately, these methods over amplify noise in homogenous sections of an image, and therefore we will use an adaptive histogram equalization that limits the contrast enhancement based on the transformation function used to change the intensities of the image before and after contrast enhancement (CLAHE). To clearly visualize each region identified by this method, we apply a 20x20 median filter on this result and then erode the image to separate loosely connected regions. Any eroded region that has an area below 40,000 pixels will be removed. The 40,000 value was discovered by experimentation with over 20 image samples, and used to remove noisy object that would be too small to be considered an object of interest. We then dilate it again so that we can attain a similar size of the region before erosion. A visual explanation of the process is shown in FIGURE 6.



Finally to help transition to the next aim, we need to apply the transformation we concluded with from the registration phase on the segmented mask extracted from the previous step of the segmentation phase, so that the segmented region now is aligned with the corresponding regions in the images taken 24 hours after experimentation.

CALCULATING CELL DEATH

Now that we have masks representing the estimated segmentation of the layers for the hippocampus 24 hours after experimentation, our final step would involve calculating the cell death within these regions. The current method used to measure cell viability in the lab is to use an imaging program, like Metamorph or ImageJ, and apply a lower limit threshold. The fluorescence images are all 16-bit images. A lower threshold value of 500 is applied on the fluorescence image as a pre-processing step, and cell death is measured. Cell death is measured as ratio of fluoresced pixels to pixel area of extracted region. We will use

Figure 6 Segmentation Process

a similar method in measuring fluorescence in this paper, with a threshold of 500 for the set of 14 slices. Figure 7 shows the steps described above before quantitative measurements are

extracted. The raw 16-bit fluorescence image of hippocampus slice is taken after experiment (Figure 7 Top Left). A threshold with a lower limit of 500 to remove fluoresced areas with less probability of major cell death is applied on the raw image (Figure 7 Top Right). The manually outlined regions is applied on the processed fluorescence image. (Figure 7 Bottom Left). Automatic segmented region is applied on the processed fluorescence image (Figure 7 Bottom Right).

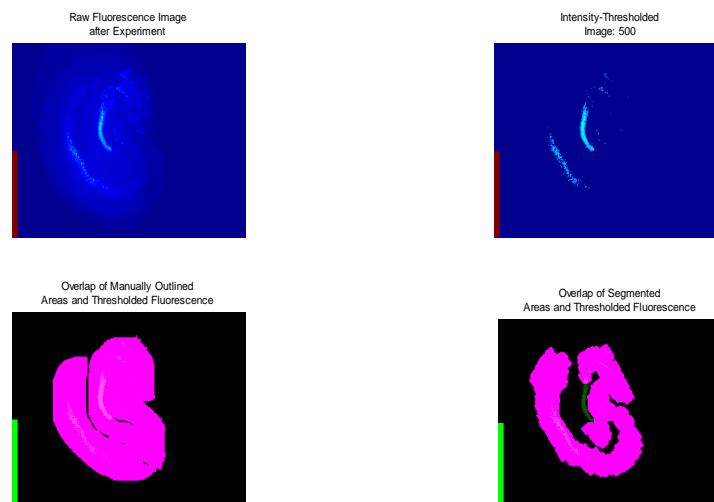


Figure 7 Fluorescence Measurement Process Shown. Raw Fluorescence image (Top Left). After threshold (Top Right). Within bottom left and right images, pink shows manually delineated regions without cell death. White shows area of cell death captured by manually delineated (Bottom Left) or automatically segmented (Bottom Right) regions. Green shows area of cell death not captured by manually delineated (Bottom Left) or automatically segmented (Bottom Right) regions. The red bar (Top Left, Right) and green bar (bottom left, right) of the images do not count as dead cells.

Results/Discussion

REGISTRATION RESULTS

Out of the 45 hippocampal samples, five samples were used for testing the different methods described in the previous section. To compare efficiency of methods, the same five samples were used for each of the methods. Precision is measured based on the element-

wise difference between the binary silhouettes of the pre and post image. The first six following methods described refer to the pre set of images as the moving images and the post set of images as the reference images to prevent losing any information related to the morphology of the hippocampus.

Affine Progression

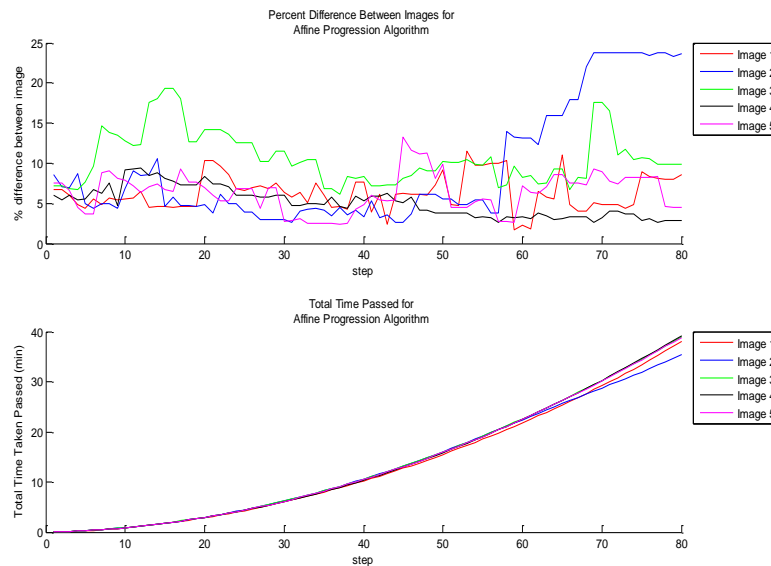


Figure [8]. Results from tests on Affine Progression method for 5 images (Top) The percent difference between the registered image and the reference image. . (Bottom) Time passed after each step in minutes, per image. (24-hour image silhouette), per image.

The first experiment involved the affine transformation type, which allows translation, rotation, scaling, and shearing of the image. According to data shown in Figure [8], the registration is not consistently improving. Because the Mattes Mutual Information registration tends to

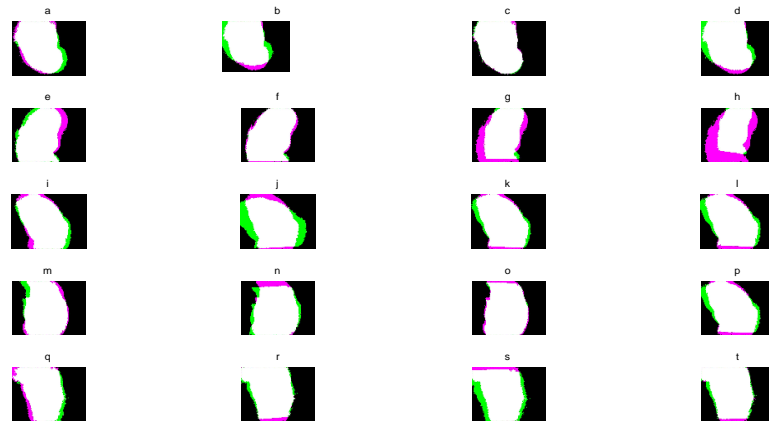


Figure [9]. Overlapping registered image on reference image for Affine Progression Method at various time points. The part of the registered image that is not overlapped by the reference image is shown in green. The part of the reference image that is not overlapped by the registered image is shown in pink. The parts of each image that do overlap are shown in white, for inside the hippocampus, and black, outside the hippocampus. The initial overlap before registration for Images 1-5 are shown in (a,e,i,m,q). The last step of the registration for Images 1-5 are shown in (d,h,l,p,t). Various in-between time points are shown for Image 1 (b,c), Image 2 (f,g), Image 3 (j-k), Image 4 (n,o) and Image 5 (r,s).

overestimate or underestimate the transformation based on the previous cycle's result, the differences tend to be sinusoidal. Image 2's registration worsens the most out of the five images, as seen in Figure [9e-h]. Because affine transformation allows for shear and scaling, the moving image shrinks to match the curvature of the silhouette towards the top of the image. Additionally, this method takes 40 minutes for completion and still does not significantly decrease the percent difference between the images.

Affine Binary Branch

To counter the drastically sharp increases in percent difference, the binary branch method

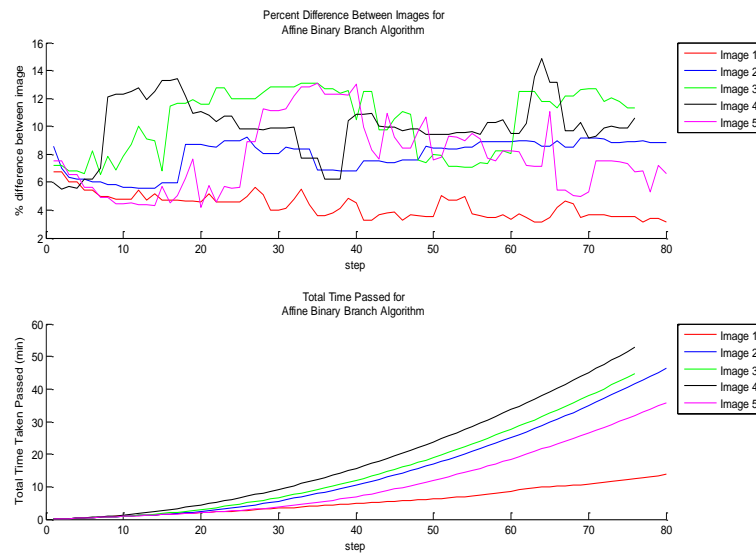


Figure [10]. Results from tests on Affine Binary Branch method for 5 images. (Left) Time passed after each step in minutes, per image. (Right) The percent difference between the registered image and the reference image. (24-hour image silhouette), per image.

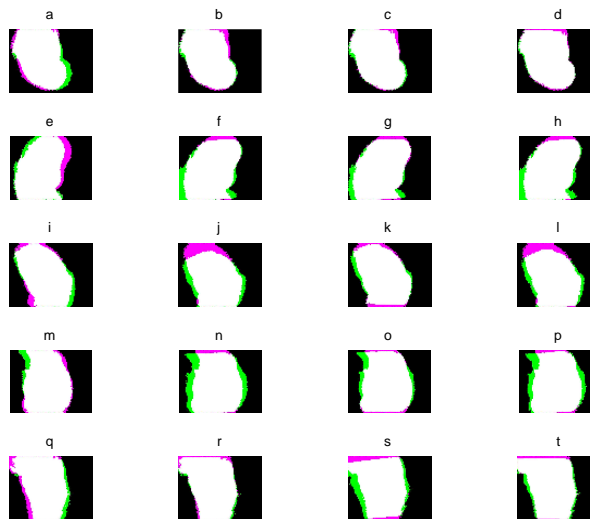


Figure [11]. Overlapping registered image on reference image for Affine Binary Branch Method at various time points. The part of the registered image that is not overlapped by the reference image is shown in green. The part of the reference image that is not overlapped by the registered image is shown in pink. The parts of each image that do overlap are shown in white, for inside the hippocampus, and black, outside the hippocampus. The initial overlap before registration for Images 1-5 are shown in (a,e,i,m,q). The last step of the registration for Images 1-5 are shown in (d,h,l,p,t). Various in-between time points are shown for Image 1 (b,c), Image 2 (f,g), Image 3 (j-k), Image 4 (n,o) and Image 5 (r,s).

was created and tested with affine transformation. As shown in Figure [10], this method was successful in avoiding drastically sharp increases because of the significant reduction of a 20% difference to one of

6%, at most. Image 1's registration, though still sinusoidal, gradually improves as the percent difference between the registered image and the reference image gradually decreases.

Unfortunately, out of the 5 images tested, this is the only registration that gradually improves. In addition, this image registration took one hour for completion, a non-ideal amount of time for the registration process. Further, it is shown in Figure [11 I,j ; m,n; r,s] that the reason why some images, such as Image 3 through Image 5, do not improve is because the silhouette is stretched or shrunk due the combination of shear and scaling factors, that is allowed in affine transformations.

Rigid Progression

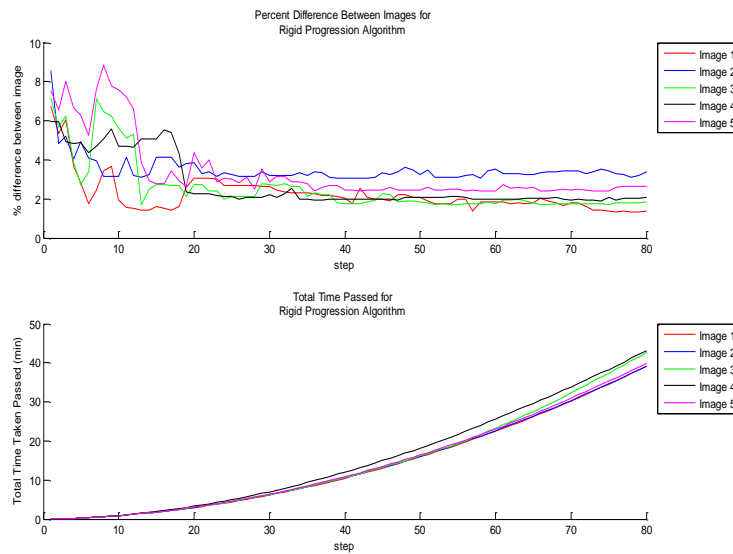


Figure [10]. Results from tests on Rigid Progression method for 5 images. (Left) Time passed after each step in minutes, per image. (Right) The percent difference between the registered image and the reference image. (24-hour image silhouette), per image.

Next, to prevent images from shearing and counter the increase in percent difference for images like Image 3 through Image 5, we change the transformation type to rigid, allowing only translation and rotation of the moving image. The progression algorithm is tested again to understand how the multimodal registration method transforms the image under this new transformation type. Figure [12] shows how all the image's registrations overall improve until

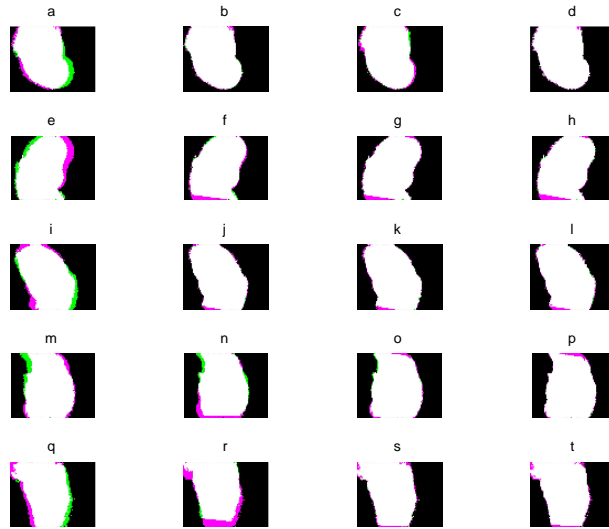


Figure [11]. Overlapping registered image on reference image for Rigid Progression Method at various time points. The part of the registered image that is not overlapped by the reference image is shown in green. The part of the reference image that is not overlapped by the registered image is shown in pink. The parts of each image that do overlap are shown in white, for inside the hippocampus, and black, outside the hippocampus. The initial overlap before registration for Images 1-5 are shown in (a,e,i,m,q). The last step of the registration for Images 1-5 are shown in (d,h,l,p,t). Various in-between time points are shown for Image 1 (b,c), Image 2 (f,g), Image 3 (j-k), Image 4 (n,o) and Image 5 (r,s).

begins, which is a drastic decrease from 40 minutes or 60 minutes in previous methods.

Figure [13] shows how the registered image is aligned with the reference image using the rigid progression method.

they reach a plateau, even though some of the image's registration worsens for a couple of steps. The plateau is reached on average 10 minutes after the registration

Rigid Binary Branch

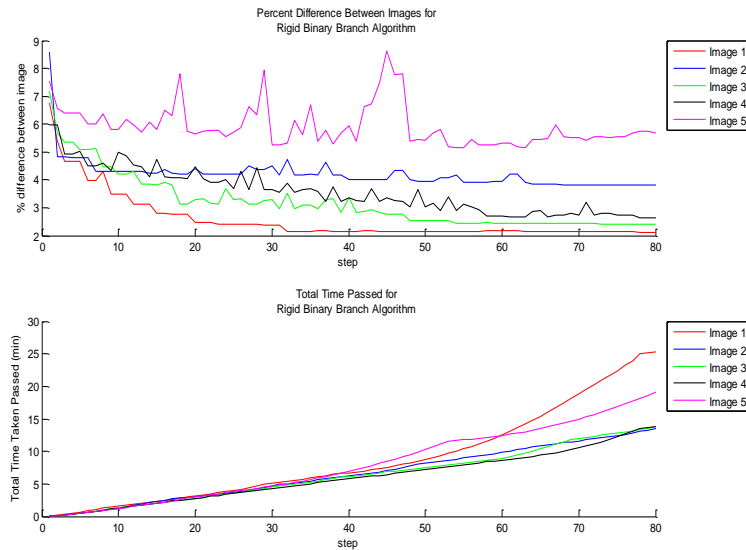


Figure [14]. Results from tests on Rigid Binary Branch method for 5 images. (Left) Time passed after each step in minutes, per image. (Right) The percent difference between the registered image and the reference image. (24-hour image silhouette), per image.

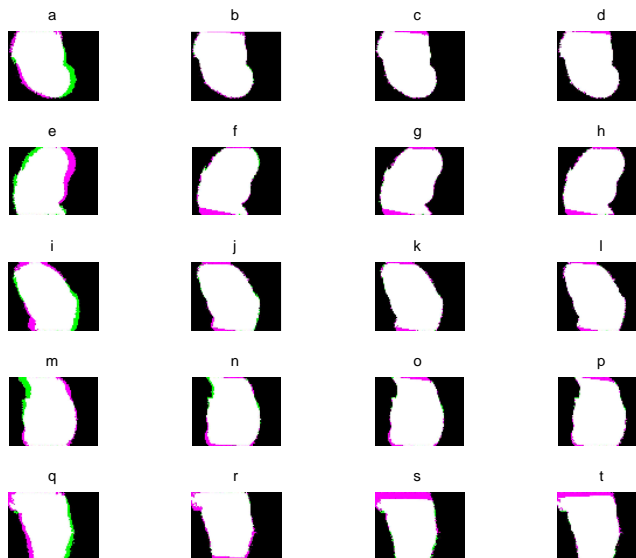


Figure [15]. Overlapping registered image on reference image for Rigid Binary Branch Method at various time points. The part of the registered image that is not overlapped by the reference image is shown in green. The part of the reference image that is not overlapped by the registered image is shown in pink. The parts of each image that do overlap are shown in white, for inside the hippocampus, and black, outside the hippocampus. The initial overlap before registration for Images 1-5 are shown in (a,e,i,m,q). The last step of the registration for Images 1-5 are shown in (d,h,l,p,t). Various in-between time points are shown for Image 1 (b,c), Image 2 (f,g), Image 3 (j-k), Image 4 (n,o) and Image 5 (r,s).

To try and improve these results and remove the temporary sharp increase or decrease in percent difference, the binary branch algorithm is combined with the rigid transformation type. According to Figure [14], registration of all images, except Image 5, improve greatly. According to Figure [15 r-t], in attempt to match both the top and the bottom of the extracted silhouette to that of the reference image, the registered image is mostly translated up and down abruptly. Because it is unable to accomplish this, the method shuffles between one image where the top of the silhouettes are aligned to another image, where the bottom of the silhouettes are aligned.

Similarity Progression

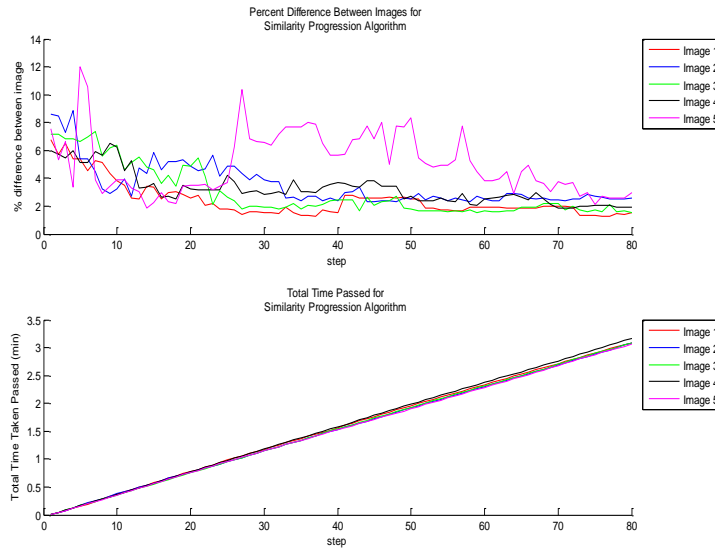


Figure [12].]. Results from tests on Similarity Progression method for 5 images. (Left) Time passed after each step in minutes, per image. (Right) The percent difference between the registered image and the reference image. (24-hour image silhouette), per image.

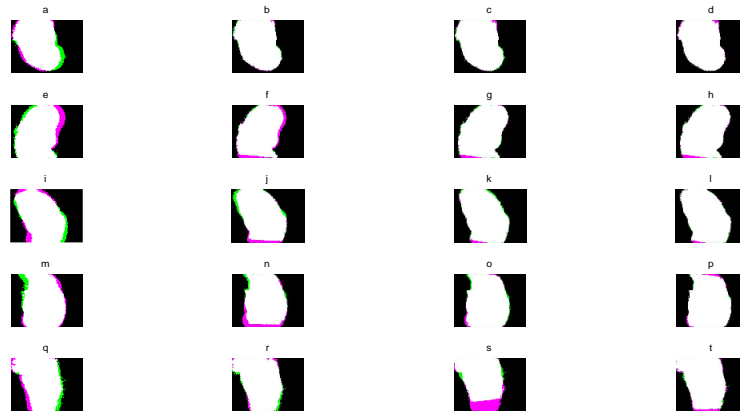


Figure [13]. Overlapping registered image on reference image for Similarity Progression Method at various time points. The initial overlap before registration for bright-field Images 1-5 are shown in (a,e,i,m,q). The last step of the registration for Images 1-5 are shown in (d,h,l,p,t). Various in-between time points are shown for Image 1 (b,c), Image 2 (f,g), Image 3 (j-k), Image 4 (n,o) and Image 5 (r,s). For the similarity transformation methods, respective bright-field images undergo the same transformation as the silhouettes to show how the actual image will appear after registration.

The similarity transformation type was attempted to account for tissue expansion between the time before experimentation and 24 hours after experimentation. This is also accounted by the fact that the areas of silhouettes are slightly different between time points,

causing the abrupt translations like in Figure [15 r-t]. As previous progression algorithm results have shown, there are large percent difference spikes in the image registrations, but the percent differences of the images using similarity transformation are equal or less than the percent differences of the previous methods. Furthermore, this method sharply decreases the time it takes to reach these values – at longest, 3 minutes.

Similarity Binary Branch

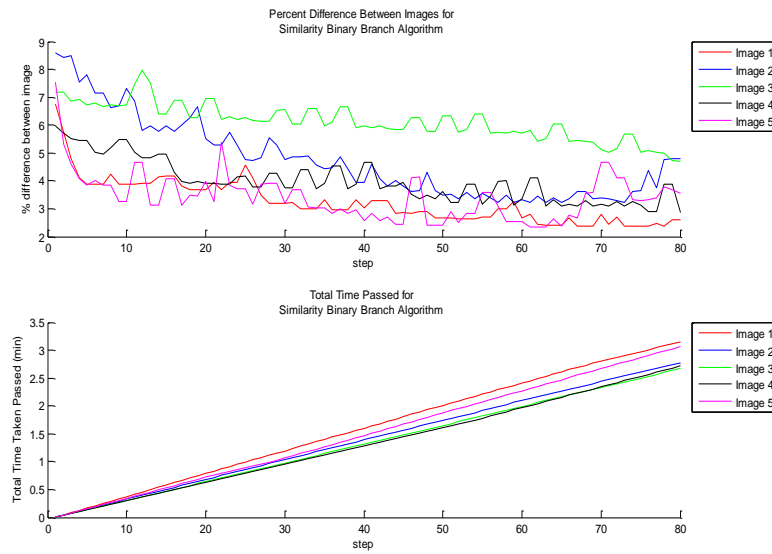


Figure [14]. Results from tests on Similarity Binary Branch method for 5 images. (Left) Time passed after each step in minutes, per image. (Right) The percent difference between the registered image and the reference image. (24-hour image silhouette), per image

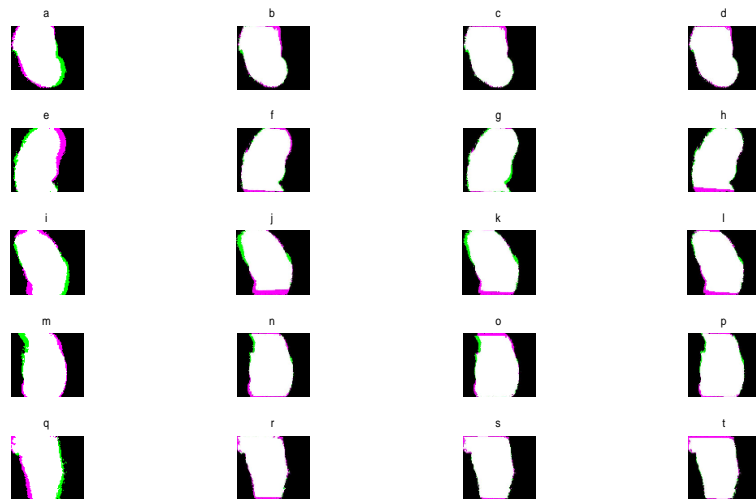


Figure [15]. Overlapping registered image on reference image for Similarity Binary Branch Method at various time points. The initial overlap before registration for bright-field Images 1-5 are shown in (a,e,i,m,q). The last step of the registration for Images 1-5 are shown in (d,h,l,p,t). Various in-between time points are shown for Image 1 (b,c), Image 2 (f,g), Image 3 (j-k), Image 4 (n,o) and Image 5 (r,s). For the similarity transformation methods, respective bright-field images undergo the same transformation as the silhouettes to show how the actual image will appear after registration.

Now that we have a method that performs faster, the binary branch algorithm is applied to a similarity transform type, in hope of removing the sharp increases in percent

difference between the registered and reference image. Figure [19 r-t] shows how Image 5's spikes from the similarity progression method are controlled, and the percent difference for Image 5 gradually decreases in this method after a sharp decrease. The total time for this process is also equal or less than the similarity progression method, proving relatively effective.

SEGMENTATION PHASE:

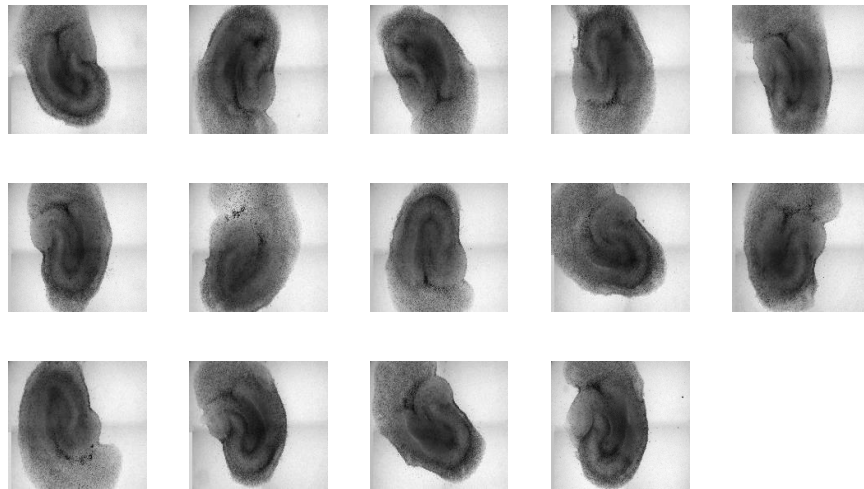


Figure 20 Raw Bright-field Images of 14 slices from 4 different rat brains

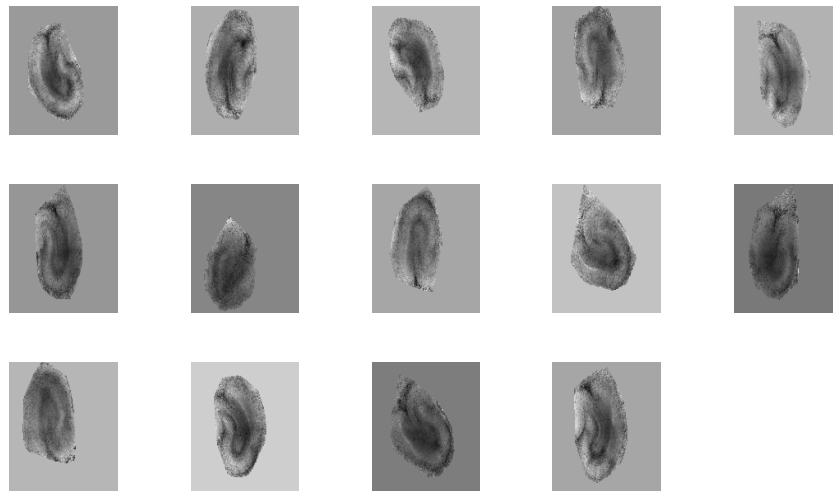


Figure 21 “Concentrated” Region of 14 slices from Figure 20. Raw images are 16-bit and their intensities are inverted so that dark regions have higher intensity. A convex hull of the top 30% of the inverted image’s intensities are extracted and applied as a mask on the raw images, giving the “concentrated” region. The background is given an intensity of the average intensity along the border of the concentrated region.

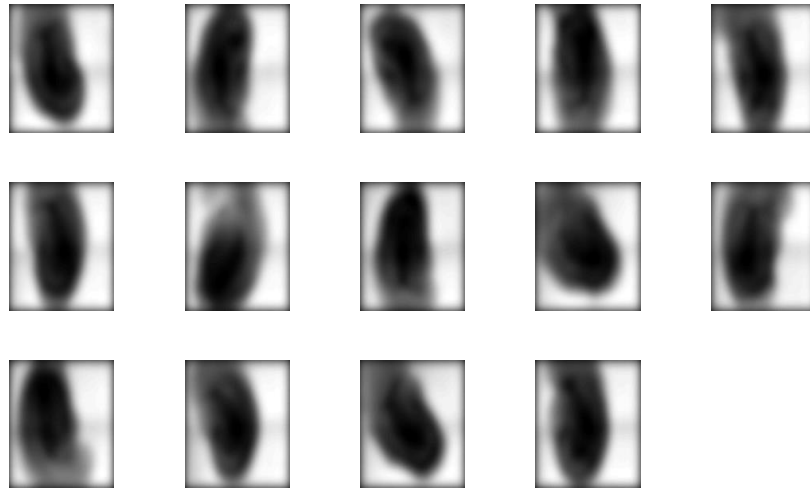


Figure 22 10 Hz Butterworth Filter and 2x2 Median Filter applied on Original Slices from Figure 20.

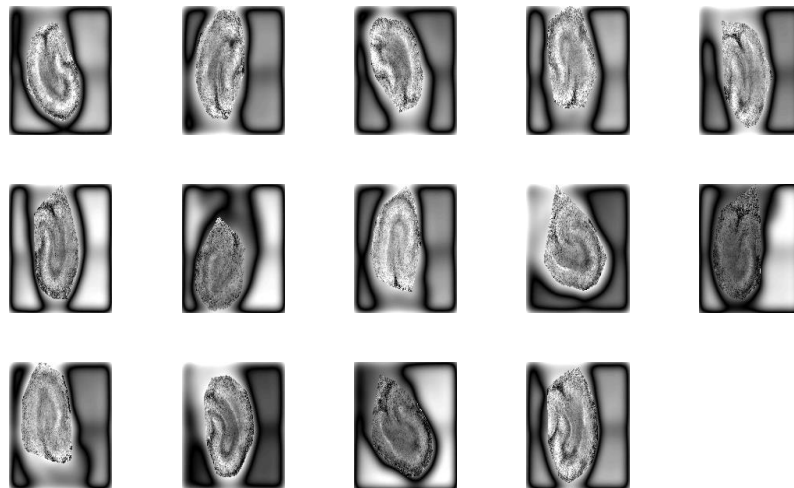


Figure 23 Images result from difference between Figure 21 and Figure 22 are extracted. The resulting images are contrast enhanced such that 1% of values are saturated at high and low intensities.

Out of the 45 hippocampal samples, fourteen samples were used for testing the accuracy of the segmentation method. Precision is measured based on the element-wise difference between the regions manually outlined and filled by an experienced user, and the regions extracted by the segmentation method. Figures 20-28 show the key steps in the segmentation process on fourteen slices.

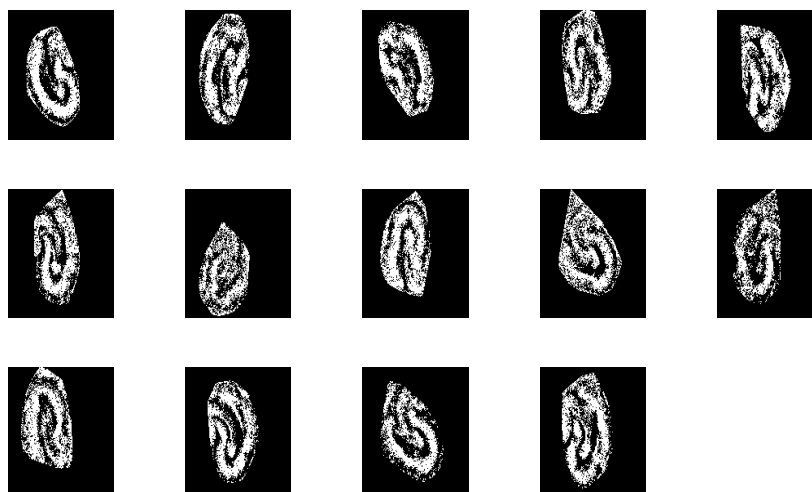


Figure 25 Scale result from CLAHE to maximum intensity

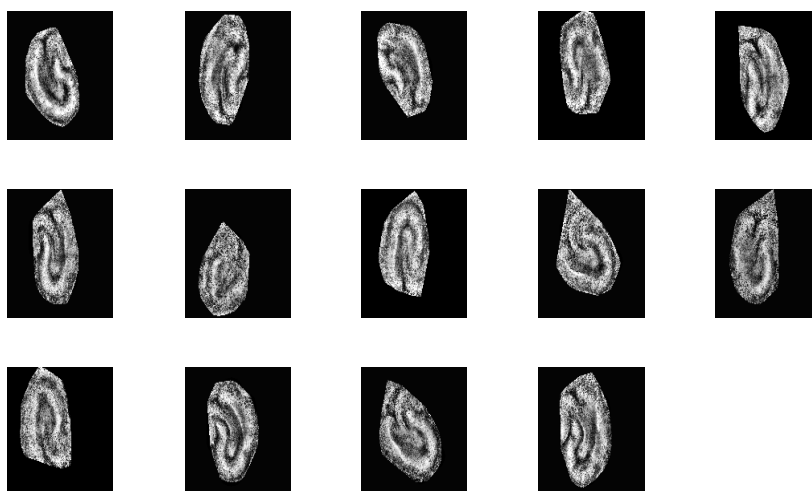


Figure 24 CLAHE contrast enhancement on resulting images of Figure 23. All regions outside the concentrated region are ignored

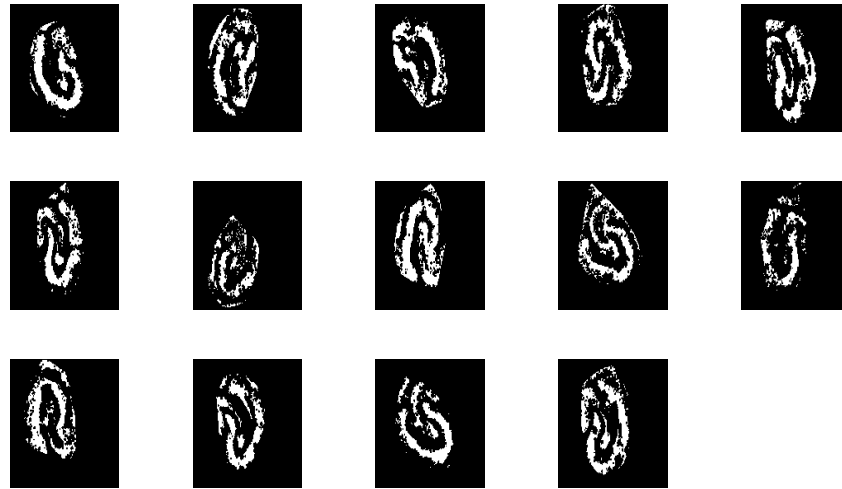


Figure 26 20x20 Median Filter to fill in small gaps in extracted regions. A 10 pixel radius disk structuring element is then used to separate loosely connected regions

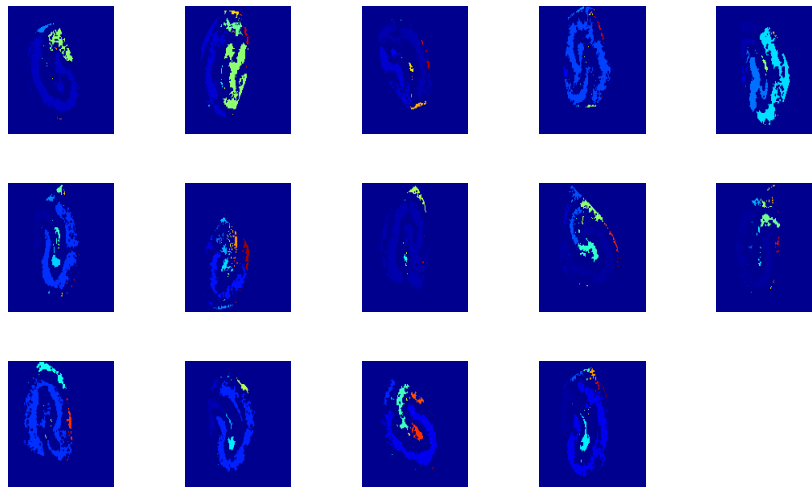


Figure 27 Different Connected Components Labeled. Segmentation process has identified DG separately from CA1,CA3 (Slice 1,7,9,10,14) while others are identify the layers all together (Slice 3,4,11).

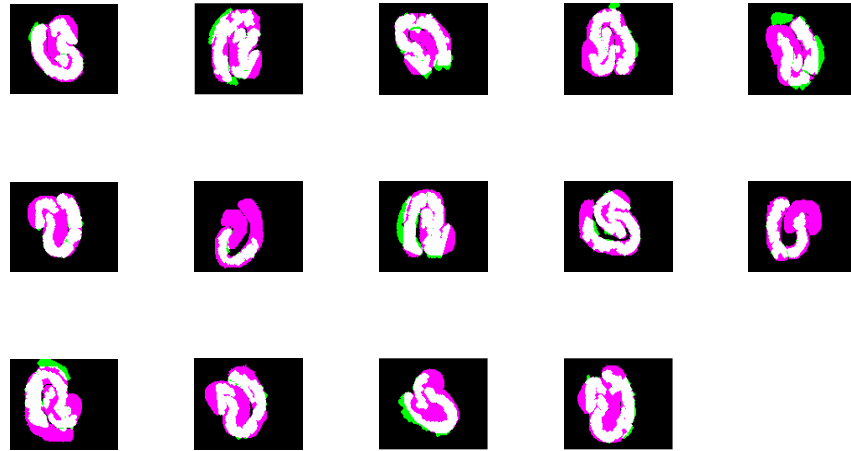


Figure 28 After removing connected components whose area were too small to be identified as a separate region, the extracted regions are shown against the regions outlined by experts, representing the standard of comparison. White areas represent regions that are covered by segmentation algorithm and standard of comparison. Pink regions represent regions the segmentation algorithm missed but are considered to be part of the ROI according the standard of comparison, and green are regions extracted by the segmentation algorithm, that are not part of the outlined regions from the standard.

Combining Segmentation and Registration

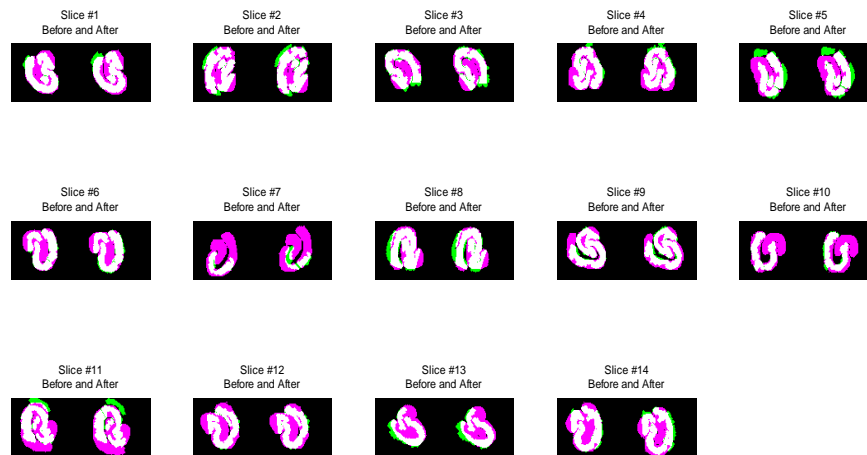


Figure 29 Target registration error. Each subplot represents a hippocampus slice showing comparison of manually outlined regions on image of slice before and after experimentation with extracted region before and after registration of hippocampus. This shows that for most of the images, with the exception of slice 7, the hippocampus regions extracted from images of slices taken after experimentation correspond to similar regions of those extracted before experimentation. Pink regions represent regions the segmentation algorithm missed but are considered to be part of the ROI according the standard of comparison, and green are regions extracted by the segmentation algorithm, that are not part of the outlined regions from the standard of comparison. White represents properly identified regions.

Now that we have our segmented regions from images of slices taken before experimentation, we need to use the transformation obtained from the registration phase for each slice to locate the corresponding regions on the images taken of slices after experimentation to provide a more accurate measurement. Out of all the tested registration methods, we decided to use the Similarity Progression method as it provides the best in both precision and efficiency over tested images. The transformation resulting from the Similarity Progression method is applied on the segmented regions obtained from raw bright-field images of slices before experimentation. An expert manually delineated the regions on the images of slices taken before experimentation and manually moved them to corresponding regions in the images taken after experimentation. The results for 14 slices on this step are shown in Figure 29.

Fluorescence measurements

Based on the segmentation masks created from automatically extracted regions, we measure cell death using images of slices taken after experimentation. Cell death in this context is calculated as the ratio between the number of fluorescent pixels within the extracted region and the pixel area of the extracted region. Results of cell death measurements are shown in Figure 30. Slices 1-4 have a minor level of injury, but because segmentation area is underestimated, important areas of minor cell death are not included in the measurement, therefore underestimating the overall cell death percentage. On the other hand, slices 5-14 have overall high level of injury, and because areas are generally

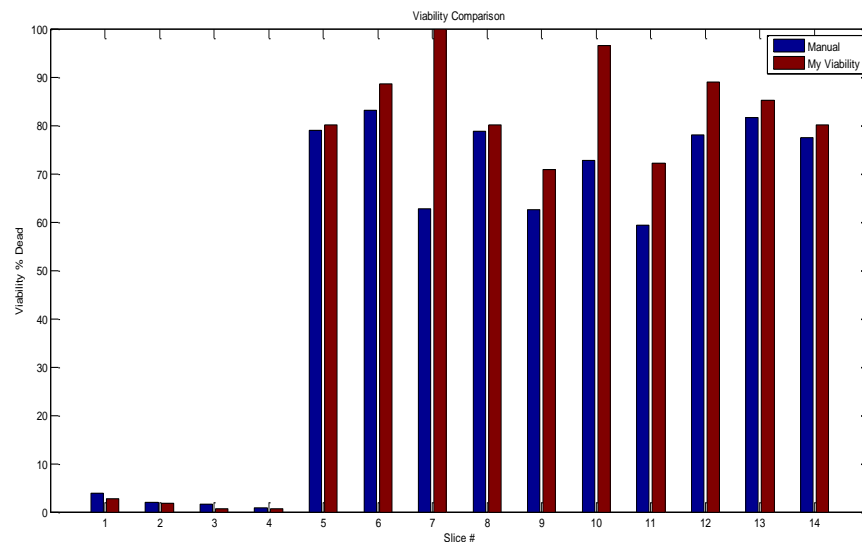


Figure 30 Cell Death Measurements for 14 slices from 4 different rat hippocampi. Values measured using Metamorph program and manually outlined regions are shown in blue. Values measured by automatic segmentation method are shown in red.

underestimated, the overall cell death percentage is overestimated. Figure 31 shows overlap of fluorescence image after threshold with automatically segmented regions, while Figure 32 shows overlap of fluorescence image after threshold with manually delineated regions. Slice 7 and slice 10's automatically extracted region are underestimated greatly, and exclude

regions with no cell death that are clearly labeled as either CA1, CA3, or DG, and therefore have automatic cell death percentage measurements at or near 100%. The boundaries of the layers can also be prone to bias, even under manual delineation, as shown with the green areas of Figure 32 (Slice 7-10).

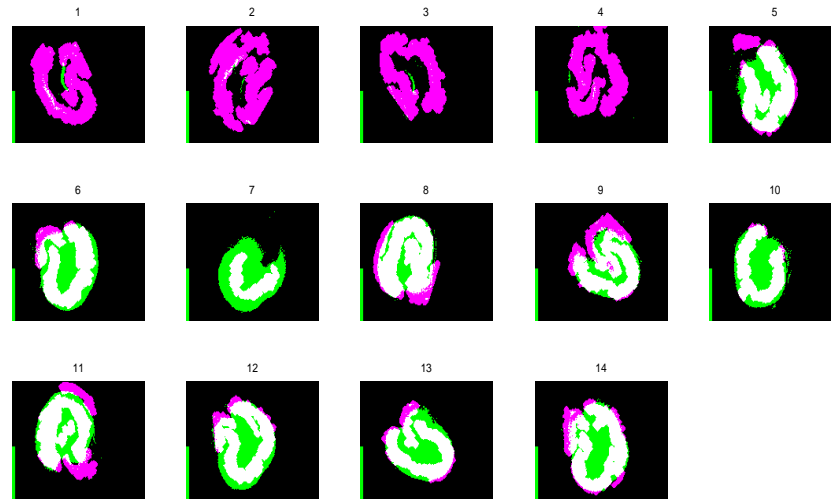


Figure 31 Overlap of Fluorescence Image after threshold and binary step and automatically segmented regions. Green represents area of cell death not picked up by segmented regions. White represents area of cell death picked up by segmented region and Pink represents region of no cell death. Regions within Slice 7 and Slice 10 are largely

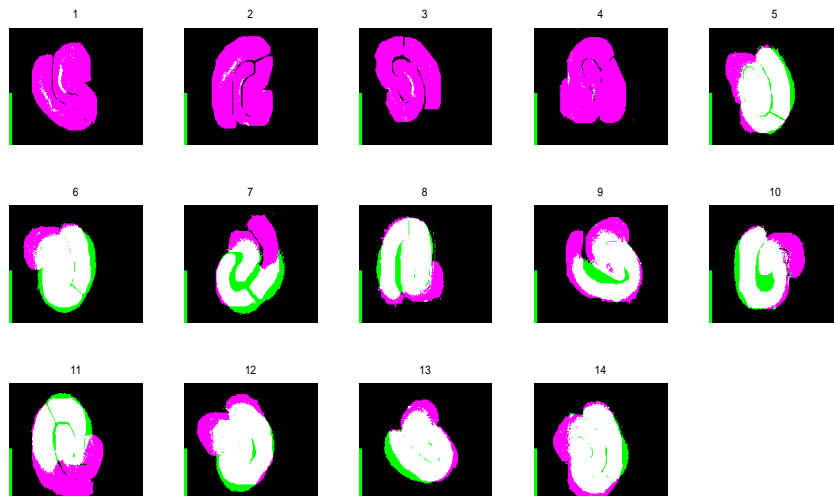


Figure 32 Overlap of Fluorescence Image after threshold and binary step and manually segmented regions. Green represents area of cell death not designated as part of CA1, CA3, or DG layers. White represents area of cell death within CA1, CA3, and DG layers and Pink represents CA1, CA3 and DG region with no cell death.

Despite the overall process, including alignment of hippocampus between time points, segmentation of hippocampus layers, and fluorescent measurements, being the same, there can be a huge difference in the cell viability measurements. This case is shown in Figure 33 which shows the results for cell death measurements from the automatic method and 2 manual experts, one using Metamorph and other using ImageJ. The huge difference in cell viability measurements between experts is due to the combination of differences in alignment and segmentation of bright-field images, along with the threshold value applied fluorescence images. For example, the main reason why the automatic method's results are closer to the manual method using Metamorph for slices 5-14 is because the threshold value applied on the images in automatic method are closer to the threshold used by the Metamorph user. Fluorescence measurements are highly susceptible to variability for images of highly injured slices. On the other hand, the automatic method's results are closer to the manual method using ImageJ for slices 1-4 because the area segmented from the images automatically are closer to the areas segmented by the ImageJ user. As stated before, for slices with little injury, it is important to segment out the regions properly or parts of the hippocampal slice that are not classified as CA1, CA3 or DG, and yet contain dead cells, will be ignored. The automatic method will provide a standard for comparison and further analysis of these slices to help come up with better ways of protecting neurons from secondary and tertiary injury.

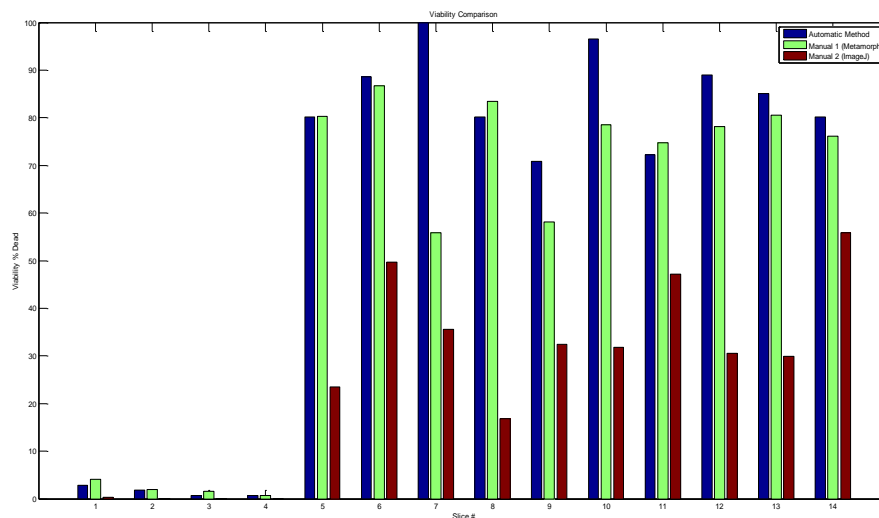


Figure 33 Cell Death Measurements for 14 slices resulting from novel automatic method and 2 manual methods, one using Metamorph, and other using ImageJ.

Now that we have taken a look at the precision of the registration, segmentation and fluorescence phase of the project, we need to validate the efficiency of this method. Figure 31 shows the time taken for the entire process from registration through fluorescence phase for the 14 test slices. The entire process was repeated five times for each image. Mean and

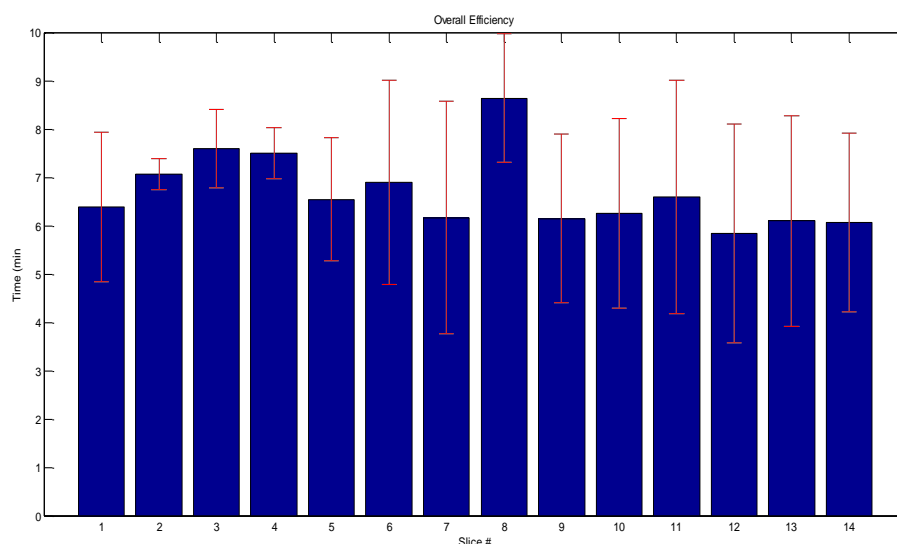


Figure 34 Efficiency of automated process from beginning of registration phase until end of cell viability measurement phase.

standard deviation times are shown in Figure 34. Overall, the entire process takes an average

of 7 minutes to finish per image, and is comparable to the time it manually outline the layers and measure cell viability manually.

Conclusion:

Based on the total of 6 registration methods discussed above on five images, the method that was the most precise and efficient is the Similarity Progression because the percent difference between the registered and reference image gradually decreases for four out of the five images to 2-3% within 3 minutes. When adding a stopping condition for diminishing returns, the efficiency increased to around 1-2 minutes. When comparing to the Metamorph user, the segmentation method underestimates the area of the regions of interest by an average of 12%, and takes an average of 3 minutes to complete. The fluorescence phase takes only about 1 minute to complete on average, therefore leading towards the 7 minutes per average overall. This is around the same amount of time for experts to use the current method per image, by manually delineating the regions of interest on the image of slice taken before experimentation, transposing it to corresponding region in images taken after experimentation, and measuring cell viability using Metamorph or ImageJ. Though there is room for improvement in efficiency, this will allow the users to save time by working on other experiments while data on cell viability is being collected. It will also prevent expert-to-expert bias when segmenting regions and measuring fluorescence.

The reason why bright-field images of slices are taken, is to help the user identify where the regions are within the hippocampus. Because of this, the bright-field images like slice 7 and 10 which have a much darker region overall even before experimentation are harder to work with it, and therefore allow for more bias when identifying layers. Because of the overall darker CA1, CA3 and DG layers, it is harder to identify by using pure intensity

gradients as the segmentation method in this paper depends on. Users can identify images that have poor quality in terms of identifying regions of interest like Slice 7 and 10 and identify regions on manually for these while having the automatic process collect cell death data on the rest of the images that are clearer. Contrast enhancement helped identify parts of the regions, but specific regions of interest were lost due to the higher difficulty in discerning layers within these images.

Because the efficiency and accuracy are dependent on the quality of the images, and how the image was taken, there are also several steps that researchers can take in order to help increase the efficiency and accuracy of the automatic method. During the experiment four slices from one hippocampus are placed in one well together. Currently the orientation of slices all differ based on how they are placed in the well. If the researcher were take images of the slices such that they were in the same orientation, or the slices were all oriented in the same direction in the well, that would allow the registration phase to apply the same transformation for every four slices, reducing the time it takes to register the images to a quarter of the current time. Considering that the registration phase is the limiting step in terms of efficiency, this would decrease the time needed for the entire process over multiple images drastically.

Our next step will be to identify and differentiate the specific layers in a hippocampus from each other, so we can further study how secondary and tertiary injury is caused and propagates, and how susceptible cells of specific regions of the hippocampus are to these types of injury. At the moment, it is possible to identify the CA1 and CA3 regions apart from the DG, but further improvement can be made to make it more robust and specific so that we can differentiate CA1 from CA3 as well.

Appendices

References:

1. Bramlett HM, Green EJ, Dietrich WD. (1997). Hippocampally dependent and independent chronic spatial navigational deficits following parasagittal fluid percussion brain injury in the rat. *Brain Res*, **762**,195–20
2. Bruns Jr J, Hauser WA. (2003). The epidemiology of traumatic brain injury: a review. *Epilepsia*, 44(Suppl. 10), 2–10.
3. Faden AI, Demediuk P, Panter SS, Vink R. (1989). The role of excitatory amino acids and NMDA receptors in traumatic brain injury. *Science*, 244, 798–800.
4. Fitzpatrick, J. Michael, Derek L. G Hill, and Calvin R. Maurer, Jr. Image Registration: Geometrical Transformation. Retrieved from <http://tango.andrew.cmu.edu/~gustavor/42431-intro-bioimaging/readings/ch8.pdf>.
5. Laurer HL, Lenzlinger PM, McIntosh TK. (2000). Models of traumatic brain injury. *Eur J Trauma*, 26, 95–110.
6. Levin HS. (1998). Cognitive function outcomes after traumatic brain injury. *Curr Opin Neurol*, **11**, 643–646.
7. Minjeong Kim, Guorong Wu, Dinggang Shen, “Unsupervised Deep Learning for Hippocampus Segmentation in 7.0 Tesla MR Images “, MICCAI Workshop on Machine Learning in Medical Imaging (MLMI 2013), Nagoya, Japan, Sep. 22, 2013
8. Morrison III, B., Cater, H. L., Benham, C. D., and Sundstrom, L. E. (2006). An in vitro model of traumatic brain injury utilizing two-dimensional stretch of organotypic hippocampal slice cultures. *J.Neurosci.Methods*, 150, 192-201.

9. R. Ali, M. Gooding, T. Szilágyi, B. Vojnovic, M. Christlieb, and M. Brady,
"Automatic segmentation of adherent biological cell boundaries and nuclei from
brightfield microscopy images", ;presented at Mach. Vis. Appl., 2012, 607-621
10. SHEN, Kai-kai. "Automatic Segmentation and Shape Analysis of Human
Hippocampus in Alzheimer ' s Disease." (2011): n. pag. Print.
11. Shi, Lin et al. "A Survey of GPU-Based Medical Image Computing Techniques."
Quantitative imaging in medicine and surgery 2.3 (2012): 188–206. Web. 6 Aug. 2014.
12. Sosin DM, Sniezek JE, Waxweiler RJ. (1995). Trends in death associated with
traumatic brain injury Success and failure. JAMA, 273, 1778–80.
13. Tscherepanow, M., Zollner, F., Hillebrand, M., Kummert,, F.: Automatic
Segmentation of Unstained Living Cells in Bright-Field Microscope Images. In:
Perner, P. Salvetti, O. (eds.) MDA 2008. LNCS (LNAI), vol 5108, 158-172. Springer,
Heidelberg (2008).
14. Ulysses, J N. "Measuring Similarity in Medical Registration." (2010): n. pag. Print.
15. Wang CC, Deng JM, Ateshian GA, Hung CT. (2002). An automated approach for
direct measurement of two-dimensional strain distributions within articular cartilage
under unconfined compression. J Biomech Eng, 124, 557–567.

Bibliography

1. A. Ardeshir Goshtasby: 2-D and 3-D Image Registration for Medical, Remote Sensing, and
Industrial Applications, Wiley Press, 2005.

2. Mateo, Juan L., and Antonio Fernández-Caballero. "Finding out General Tendencies in Speckle Noise Reduction in Ultrasound Images." *Expert Systems with Applications* 36.4 (2009): 7786–7797. Web. 21 July 2014.
3. Morrison III, B., Cater, H. L., Benham, C. D., and Sundstrom, L. E. (2006). An in vitro model of traumatic brain injury utilizing two-dimensional stretch of organotypic hippocampal slice cultures. *J.Neurosci.Methods*, 150, 192-201.